Detrick, R., Honnorez, J., Bryan, W. B., Juteau, T., et al., 1990
Proceedings of the Ocean Drilling Program, Scientific Results, Vol. 106/109

5. PETROSTRUCTURAL ANALYSIS OF THE LEG 109 SERPENTINIZED PERIDOTITES[1]

Mathilde Cannat,[2] Thierry Juteau,[2] and Emmanuel Berger[3]

ABSTRACT

The serpentinized peridotites at Site 670 have a harzburgitic to lherzolitic protolith. They have been deformed plastically at high temperature and moderate deviatoric stress conditions typical of the mantle. They have subsequently been serpentinized in static conditions. The dip of the plastic foliation and the plunge of the lineation vary significantly downhole. This suggests either that the rocks recovered come from large shear polyhedra of serpentinized peridotite, which preserved their mantle structures, but rotated in a matrix of sheared serpentinite, or that Site 670 is set on a heap of dekametric blocks, fallen from a serpentinite cliff nearby. The possible modes of emplacement of the serpentinized peridotites on the seafloor of the median valley wall are discussed. A model involving tectonic stretching of a thin magmatic crust is favored.

INTRODUCTION

The serpentinized peridotites were recovered at DSDP Site 670, about 5 km west of the central volcanic axis of the Mid Atlantic Ridge (M.A.R.), and some 45 km south of the Kane Fracture Zone (Fig. 1). This site lies in the "complex transition zone" defined by Detrick and Purdy (1980) and Cormier et al. (1984) between a seismic crust of "normal thickness" (~6 km) to the south, and a thinner seismic crust (~4 km) to the north. The serpentinite body drilled at Site 670 may extend northward over more than 20 km, as serpentinites were also recovered west of DSDP Site 649 (Fig. 1) by the submersible *Alvin* (Karson et al., 1987). In addition, plastically deformed serpentinites, with a harzburgitic protolith, were drilled during Leg 45 at DSDP Site 395, located about 100 km west of the M.A.R. volcanic axis (anomaly 4; Shipboard Scientific Party, 1979).

We examined 43 samples (42 serpentinized peridotites and 1 websterite), from the 9 cores covering the 92.5-m-deep drill hole (Fig. 2A). 8 samples (1 in Core 3, 5 in Core 5, 1 in Core 6, and 1 in Core 8; Fig. 2B) are "oriented"; in these samples, the vertical is known. Recovery rates ranged from 1.2% to 17% (Fig. 2B). Because of this very low recovery, the absolute depth of provenance of a given sample is not known.

All the studied samples are tectonites: elongated spinel and orthopyroxene grains define a foliation and a lineation. These structures are sometimes visible directly on the cored section; this is the case for the subhorizontal trace of the foliation in Core 6 (Figs. 2D and 3). In most samples, however, the attitude of the foliation and lineation can only be ascertained through detailed microstructural analysis; this is one of the aims of the following study. The petrostructural analysis also reports on: (1) the relative chronology of the deformation, crystallization, and recrystallization events observed in the serpentinites; (2) the temperatures and deviatoric stresses prevailing during the deformation; and (3) the coaxial or noncoaxial character of the strain regime and the relative strain intensities. These data are used to discuss the mechanics of emplacement of the serpentinites into their present crustal position. The petrogenetic history of the serpentinites is detailed and discussed in a companion paper by Juteau et al. (this volume).

PETROGRAPHY AND MICROSTRUCTURES

The Serpentinized Peridotites

The modal composition of the serpentinized peridotites indicates that their protolith ranged from dunitic to lherzolitic. Table 1 gives the modal composition of the nine samples (eight serpentinized peridotites and one websterite) selected for a detailed investigation of their primary mineralogy (see Juteau et al., this volume). These modal compositions were obtained by counting a minimum of 1000 points by section, on a grid spacing of 0.05 mm. The mineral phases taken into account are olivine (ol), orthopyroxene (opx), clinopyroxene (cpx), and Cr-spinel (sp) for the primary phases, and serpentine, bastite, talc, tremolite-actinolite, and magnetite for the secondary phases. The reconstructed primary modes were calculated with the following conventions: (1) mesh-textured serpentine and associated magnetite grains were assigned to primary olivine; (2) bastite pseudomorphs and associated talc were assigned to primary orthopyroxene; (3) tremolite-actinolite clusters or rims were assigned to both primary orthopyroxene and clinopyroxene; and (4) magnetite developed at the margins of Cr-spinels was assigned to primary spinel. The calculation of these primary modes does not take into account the volume increase associated with serpentinization. Thus, they overestimate the modal proportions of olivine and orthopyroxene, and underestimate the clinopyroxene and spinel. A probably more accurate estimate of the clinopyroxene modal contents is also presented in Table 1. It is calculated assuming a volume increase of 30% when serpentinization is complete (Nicolas, 1969; Komor et al., 1985), and a linear volume increase with increasing serpentinization. These corrected clinopyroxene contents range from 0.7% to 16.9% in the eight selected serpentinized peridotite samples. This wide range of values illustrates the fact that the clinopyroxene is not evenly distributed in the serpentinites. Instead, it concentrates, with associated orthopyroxene, in clusters 1–10 mm across. These clusters are elongated in the foliation of the samples, and are present all through the core. The highest clinopyroxene modal contents presented in Table 1 were obtained for "thin-section-sized" samples including one of these pyroxene-rich clusters. The modal composition of these samples should therefore not be extrapolated to a larger volume of rock.

[1] Detrick, R., Honnorez, J., Bryan, W. B., Juteau, T., et al., 1990. *Proc. ODP, Init. Repts.*, 106/109: College Station, TX (Ocean Drilling Program).
[2] GIS Océanologie et Géodynamique, UBO, 6 ave Le Gorgeu, 29287 Brest, France.
[3] Ecole des Mines, 35 rue St. Honoré, 77305 Fontainebleau, France.

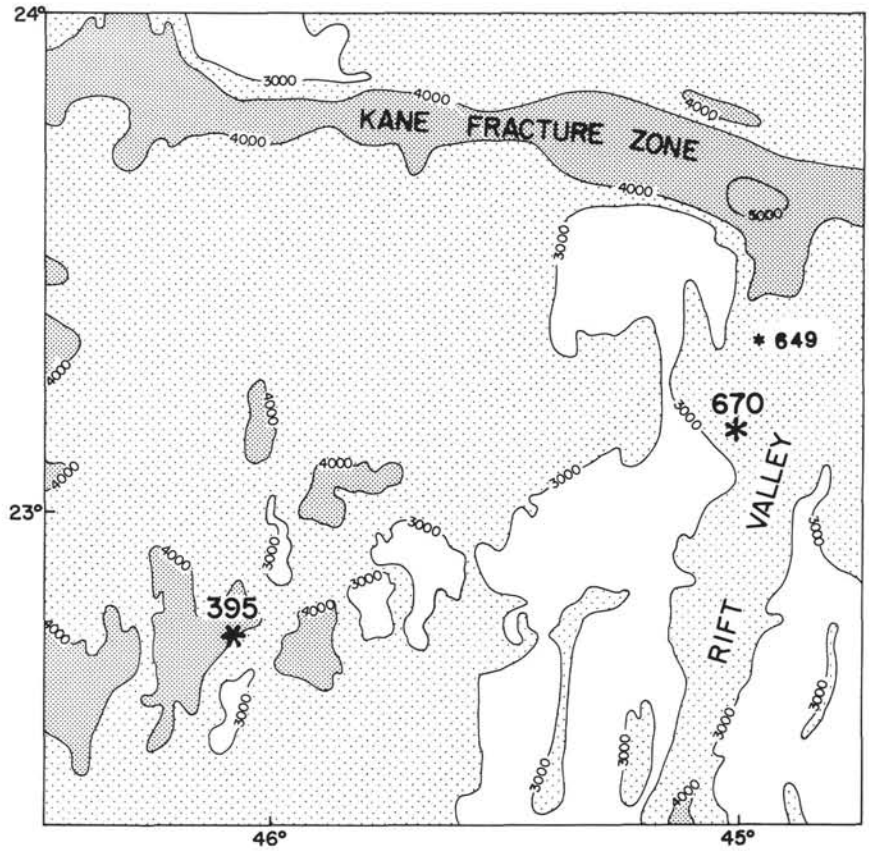

Figure 1. Location map for Site 670. Serpentinized peridotites were also drilled at Site 395, during DSDP Leg 45, and sampled on the median valley wall west of Site 649, by the *Alvin* (Karson et al., 1987).

The microstructure of the serpentinized peridotites is of the "elongated porphyroclastic" type (Mercier and Nicolas, 1975). The foliation and lineation are defined by the alignment of spinel grains (Figs. 3 and 4A) and by the elongation of porphyroclastic orthopyroxenes (0.5–1.5 cm) and olivines (0.1–1 cm).

Estimates (with the optical microscope) of the degree of serpentinization in the 43 studied samples show that the samples from Cores 1, 2, and 3 (6.4–35.7 m) are 80%–100% serpentinized (Fig. 2C). Highly serpentinized peridotites are also found in Core 5 (45.2–54.6 mbsf), Core 7 (64–73.5 mbsf) and Core 9 (83–92.5 mbsf). The other studied samples are 50%–75% serpentinized (Fig. 2C). The mean serpentinization of the peridotites drilled at Site 670 may however be higher, as it is possible that the most serpentinized material was preferentially washed away during the coring operations. The serpentinization appears static in all the samples studied. An undeformed serpentinite mesh encloses relicts of olivine and pyroxene, which preserve their higher-temperature, pre-serpentinization, deformation fabrics.

Orthopyroxene

The plastically deformed orthopyroxene porphyroclasts often contain lamellar exsolution of clinopyroxene. Their [100] crystallographic planes tend to lie close to the foliation plane (Figs. 5 and 6A), and their [001] axes are close to the lineation (Fig. 6A). The [001] (100) slip-system is the easiest and most usually activated slip-system in pyroxenes (Nicolas and Poirier, 1976). Thus, the (100) cleavage of an orthopyroxene porphyroclasts is parallel to the shear plane in this crystal (Fig. 5). The preferred orientation of this cleavage in a given sample is always slightly oblique to the foliation; the deformation had therefore a noncoaxial component (see Bouchez et al., 1983). The rotational nature of the deformation is further evidenced by the development of "retort-shaped" orthopyroxenes (Figs. 4B and 6B); porphyroclasts badly oriented for slip are bent toward a more favorable position (Etchecopar, 1974).

Some orthopyroxene porphyroclasts are kinked, and partly recrystallized, with polygonal neoblasts smaller than 0.2 mm (Figs. 4B and -C).

Olivine

The olivine porphyroclasts are partly recrystallized in subpolygonal neoblasts (Fig. 5). The typical size of these neoblasts ranges from 0.2 to 0.4 mm. The one exception is a sample from Core 9 (83–92.5 mbsf), where all the olivine grains are rounded and about 1 mm in size. Neoblasts smaller than 0.1 mm are locally found, associated with recrystallized pyroxenes, in the most deformed samples (Fig. 4D).

The olivine crystallographic preferred orientation (porphyroclasts and neoblasts) is strong (Figs. 6 and 7B, -C, and -D) and corresponds to slip along the [100] axis, on several (0kl) planes. Such slip-systems are activated during high temperature deformation experiments at moderate (<1 kbar) and high (>1 kbar) stresses (see synthesis in Gueguen and Nicolas, 1980). In some samples, the dominant slip plane is (001) (Figs. 7C and -D): the [010] maximum lies close to the foliation, and the preferred orientation of the [100] axes of orthopyroxenes (or pole to the slip-plane) is similar to that of the [001] axis in olivine (Fig. 7C). The [100] (001) slip system has been activated also at high temperatures, during creep experiments at

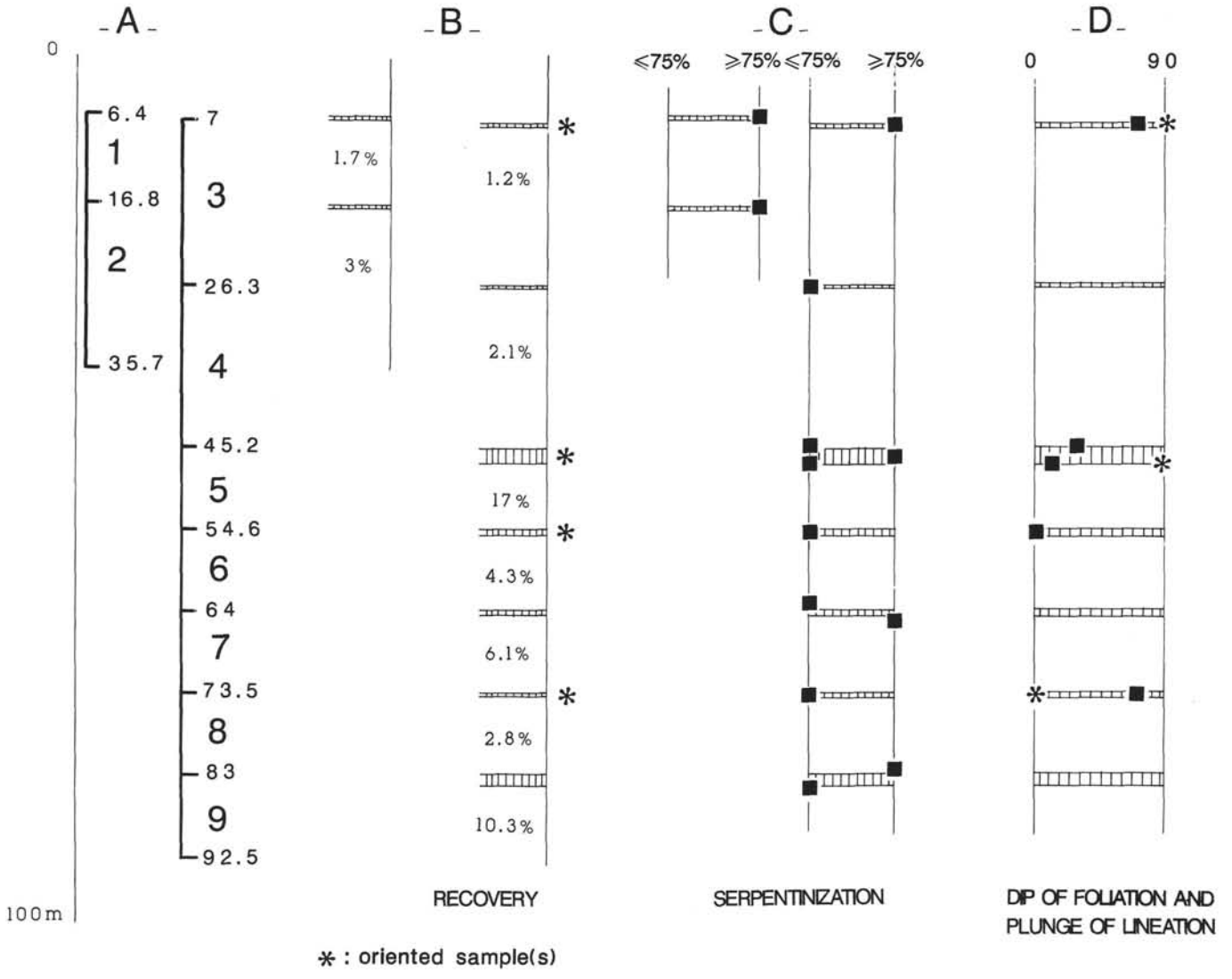

Figure 2. Elements of stratigraphy at Site 670. **A.** Stratigraphic position of each core. **B.** Rock recovery and approximate location of the "oriented" samples. **C.** Estimated degree of serpentinization (see text). **D.** Dip of the foliation shown by black squares and plunge of the stretching lineation shown by stars in the "oriented" samples (see text for explanation).

moderate stress (<1 kbar; Durham et al., 1977; Jaoul et al., 1979).

As observed for orthopyroxenes, the olivine slip plane is slightly oblique to the foliation (Figs. 6 and 7B, -C). This confirms the rotational nature of the deformation regime.

The dislocation pattern (Fig. 4E), decorated using the oxidation technique of Kohlstedt et al. (1976), consists of [100] screw dislocations crossing from one (100) tilt wall to the next; a pattern common to olivine deformed in high temperature (mantle) conditions (Gueguen and Darot, 1980). The mean spacing between the (100) tilt walls ranges from 8 to 17 μm in the four samples selected for decoration. The dislocation pattern is identical in the olivine porphyroclasts and in the smaller polygonal neoblasts. This indicates that partial recrystallization was achieved before the end of the plastic deformation (syntectonic recrystallization).

Clinopyroxene

The clinopyroxene is found as (Fig. 5): (1) small exsolved crystals along the (100) cleavages, or in fractures, of the orthopyroxenes; (2) porphyroclasts with lamellar exsolutions

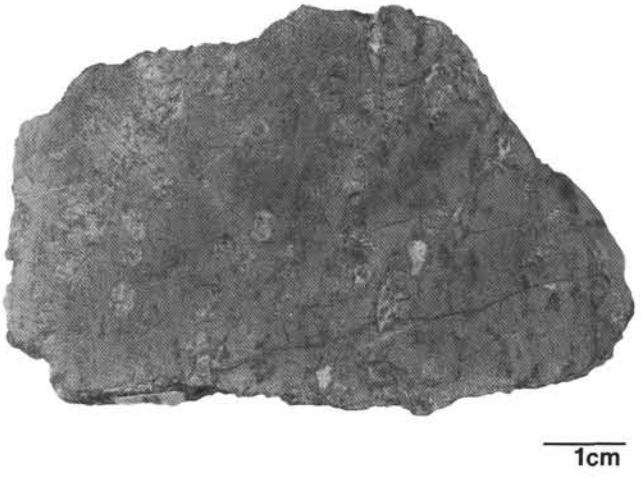

Figure 3. Sample 109-670A-6R-1 (1–10 cm). The top of the sample is at the left. The subhorizontal trace of the foliation is marked by elongated orthopyroxene and spinel grains.

Table 1. Modal analyses of nine samples from Hole 670. The primary modal proportions, calculated not taking into account the volume increase during serpentinization, are shown in parentheses. The modal proportion of clinopyroxene, taking this volume increase into account, are shown between double parentheses. Rock type: H = harzburgite; L = lherzolite; D = dunite; and W = wehrlite.

Sample	Ol	Opx	Cpx	Spin	Serp	Amph	Rock type
4R-1 (#3) 19–21 cm	12.4 (82.9)	5.2 (12.4)	3.0 (4.0) ((4.9))	0.6 (0.6)	75.4	3.3	H
5R-1 (#1) 2–6 cm	15.4 (68.7)	6.2 (15.3)	12.2 (14.5) ((16.9))	1.4 (1.4)	57.1	7.6	L
5R-2 (#12) 92–94 cm	13.0 (79.6)	1.1 (14.0)	3.0 (4.9) ((6.0))	1.4 (1.4)	74.9	6.5	H–L
5R-2 (#19) 142–145 cm	19.4 (69.6)	11.8 (19.6)	1.0 (3.0) ((3.5))	7.7 (7.7)	58.9	2.0	H
6R-1 (#6) 40–41 cm	30.8 (76.0)	4.6 (14.4)	7.6 (8.3) ((9.6))	1.2 (1.2)	53.5	2.2	L
6R-1 (#8) 49–51 cm	27.1 (79.4)	5.4 (12.3)	6.1 (7.5) ((8.8))	0.8 (0.8)	59.2	1.4	L
7R-1 (#2) 7–10 cm	22.1 (99.4)		0.6 (0.6) ((0.7))	tr	77.3	—	D
7R-1 (#3) 17–18 cm	12.7 (77.5)	4.9 (17.0)	2.7 (4.8) ((5.8))	0.7 (0.7)	71.9	7.0	H–L
9R-1 (#3) 19–20 cm	10.6 (12.0)	33.2 (42.2)	38.1 (45.7) ((46.0))	0.1 (0.1)	2.9	15.	W

of orthopyroxene, often kinked and fractured (Fig. 4D); (3) small polygonal neoblasts recrystallized around the kinked porphyroclasts (Fig. 4D); and (4) crystals smaller than 0.1 mm, in an interstitial position (Figs. 4F, -G).

In some samples, the small interstitial clinopyroxenes concentrate in lenses parallel to the shear plane (Figs. 4F, -G, and 5), as defined by the preferred orientation patterns of olivine and orthopyroxene (Fig. 6). This disposition recalls that of feldspathic lenses in the Lanzo (Boudier and Nicolas, 1972) or Trinity (Le Sueur et al., 1984) lherzolites, where it is attributed to feldspar crystallization from a circulating melt, before the end of the plastic deformation (Boudier and Nicolas, 1972; Nicolas and Jackson, 1982). A similar origin is tentatively proposed for the small interstitial clinopyroxenes of the Leg 109 peridotites. This hypothesis will be discussed in the companion paper (Juteau et al., this volume), in view of the mineralogical data.

Spinel

The spinel grains (0.05–3 mm) are reddish brown and either rounded (Fig. 4A), or wormlike ("holly leaf" type), and locally intergrown with orthopyroxene grains (Fig. 4H). Both types are elongated in the samples foliation and rimmed by secondary magnetite.

The Websterite

The websterite sample (Fig. 4I) is only slightly serpentinized (2.9%; Table 1). It is composed of 12% modal olivine, 42% modal orthopyroxene, 46% clinopyroxene, and of rare and small (~0.02 mm) euhedral spinel grains. The olivine is plastically deformed and displays subgrain boundaries. The pyroxene porphyroclasts are kinked and recrystallized in small (<0.3 mm) polygonal neoblasts. The shape fabric of these porphyroclasts defines a rough foliation. Thus, the websterite was involved in the plastic deformation affecting the surrounding peridotite.

GEOMETRY OF THE DEFORMATION

The dip of the foliation and the pitch of the lineation (Fig. 2D) were determined on the "oriented" specimens through direct observation and microstructural analysis of oriented thin sections. This approach is largely based on the observation (see previous paragraphs) that the intracrystalline slip plane (shear plane) and slip direction lie at a small angle to, respectively, the foliation and the lineation. The attitude of these structures can therefore be estimated from mineral preferred orientation measurements, when direct observation is impossible (sample too small and/or too serpentinized).

The oriented sample from Core 3 is 100% serpentinized, but the elongation of the bastite pseudomorphs marks the trace of a subvertical foliation (Fig. 7A). The preferred orientation of the greatest refractive index (or long axis of the serpentine fibers) of these pseudomorphs (Fig. 7A) may reflect that of the [001] axis, or slip direction, of the original orthopyroxenes. If this is the case, the stretching lineation in this sample is also subvertical (Fig. 2D).

In Core 5, the dip of the foliation, directly visible on the core section, does not exceed 35° (Fig. 2D). In the one moderately serpentinized oriented sample, the preferred orientation of the [100] axis, or slip direction, of the olivine (Fig. 7B) is downdip; the stretching lineation presumably lies at a small angle from this slip direction.

In the oriented samples from Cores 6 and 8, the dominant slip-plane in olivine is (001) (Figs. 7C, -D). The shear plane in these samples can therefore be drawn. It is perpendicular to the [001] maximum and it contains the [100] maximum, or slip direction.

In Core 6, the trace of the foliation, visible in thin section, is subhorizontal (Fig. 2D). The foliation itself must lie close to the shear plane (Fig. 7C), and the lineation close to the [100] maximum (slip direction). Thus, the foliation and lineation in this core are subhorizontal (Fig. 2D).

In Core 8, the subvertical trace of the foliation is visible in thin section. The shear plane is also subvertical (Fig. 7D), and the maximum concentration of the [100] slip direction in olivine (Fig. 7D) is subhorizontal. This suggests that the plunge of the lineation is small (Fig. 2D).

The foliation dips and lineation plunges deduced above vary significantly from one core to another (Fig. 2D). This geometrical variability will be discussed in the conclusion of this paper.

PHYSICAL CONDITIONS OF THE DEFORMATION

Deformation Regime

The systematic obliquity between the shear plane and the foliation (Figs. 5, 6A, -B, 7B, -C) and the presence of "retort-shaped" orthopyroxene porphyroclasts (Figs. 4B and 6B) show that the strain regime had a noncoaxial, or simple shear component.

Strain Intensity Estimates

In the XZ plane of the finite deformation frame (perpendicular to the foliation and parallel to the lineation), the maximum elongation ratio of the orthopyroxene porphyroclasts does not usually exceed 1:5. However, this ratio reaches 1:20 in a sample from Core 2 (16.8–35.7 mbsf) and 1:10 in a sample from the bottom of Core 5 (45.2–54.6 mbsf). These high elongation ratio reflect localized higher strain. Away from these higher strain intervals, the strain intensity,

as evidenced by the orthopyroxene elongation, appears roughly homogeneous.

The intensity of a simple shear deformation (γ) may be estimated through measurements of the angle (α) between the shear plane and the foliation ($\gamma = 2 \cot 2\alpha$). In the samples studied, α ranges from 10° to 20°, yielding γ values between 2.4 and 5.5. The major weakness of these estimates is that even a small pure shear component will significantly reduce α, and lead to a gross overestimate of γ.

The elongation ratio of the orthopyroxene porphyroclasts can also be used to estimate the strain intensity, assuming: (1) that the original shape of the grains was roughly equant; (2) that the orthopyroxene did not rotate in the olivine matrix; and (3) that the orthopyroxene deformed only by intracrystalline slip and did not recrystallize. The third assumption at least is obviously wrong (see Fig. 4C), and this method therefore probably leads to underestimating the bulk strain. However, for a simple shear deformation, the orthopyroxene elongation ratio lead to values around 2 in most samples, and around 4 in the deformation bands, roughly in accord with the estimates based on the angle α.

Deviatoric Stress Intensity Estimates

Experiments in steady state plastic deformation (creep) of olivine show that both the spacing (d) between the (100) dislocation walls (Fig. 4E), and the size (D) of neoblasts created during syntectonic recrystallization, decrease when the applied deviatoric stress (σ) increases. Experimental calibrations of these relations have been published by Goetze (1975), Durham et al. (1977), Mercier et al. (1977), Post (1977), and Ross et al. (1980).

These relations may be applied to the neoblast sizes measured in the Leg 109 serpentinized peridotites (D = 0.2–0.4 mm), if we assume that steady state flow conditions were reached during the deformation. These relations yield deviatoric stresses of 0.3–0.8 kbar. The mean size (1 mm) of the rounded olivines in the texturally exceptional sample of Core 9 (see above) corresponds to stresses between 0.2 and 0.35 kbar.

The spacing between dislocation walls (d = 8–17 μm) is the same in the porphyroclasts and in the recrystallized olivine neoblasts. In the rounded olivine of Core 9, the average d value is 10 μm. The σ-d relations proposed by Goetze (1975) and by Durham et al. (1977) lead to σ between 0.6 and 2.1 kbar. The σ-d relation of Ross et al. (1980) yields much higher values (2.2–7.5 kbar). This discrepancy can be due to experimental imprecision, or to the fact that several σ-d relations may exist, depending for example on the grain size, or on the strain rate (Gueguen and Darot, 1980). In any case, this discrepancy indicates that the spacing between dislocation walls is not a reliable paleopiezometer.

Temperature

The microstructures of the samples, the slip-systems activated in olivine and orthopyroxene, the syntectonic recrystallization of these minerals, all point to high temperature (≥1000°C) mantle conditions. This is in good agreement with the equilibrium temperature (~1100°C) deduced from the mineralogical study of the anhydrous phases in the peridotites (Juteau et al., this volume).

CONCLUSIONS AND DISCUSSION

The Site 670 peridotites underwent an episode of pervasive plastic deformation with a simple shear component. The finite shear strain and the deviatoric stress were probably moderate. The finite shear strain appears roughly homogeneous, and is estimated between 2 and 5, assuming a true simple shear regime. The deviatoric stress is estimated below 1 kbar, assuming steady state flow during the deformation. The slip systems activated in olivine suggest that the deformation occurred at temperatures in excess of 1000°C. This is confirmed by the mineral chemistry of the primary phases (Juteau et al., this volume). These conditions of deformation: high temperatures, moderate deviatoric stresses, and homogeneous strain are interpreted as characteristic of plastic flow in the asthenospheric mantle. In the lithospheric mantle, the temperature decreases upward, the yield stress of olivine increases, and discrete high strain intervals are likely to develop. Below about 700°C (at geologic strain rates), the olivine tends to deform in a brittle fashion (see synthesis in Kirby, 1985), producing cataclastic intervals. The serpentinization begins below about 500°C, if water is available, and serpentinite shear zones accommodate the deformation. During its ascent in the lithosphere, the peridotite body of Site 670 was surely subjected to differential stresses. According to the rheological behavior described above, these differential stresses would have successively caused nonpervasive plastic deformation, cataclastic deformation, and deformation along serpentinized shear zones. The local plastic strain concentrations observed in a few samples is evidence for a limited nonpervasive plastic deformation, but the serpentinized peridotites recovered at Site 670 are not cataclastic and were not deformed after their serpentinization. Thus, either Hole 670 did not cross any cataclastic or serpentinized shear zones, or it did and the corresponding material was washed away during the coring operations. This last hypothesis fits the very poor recovery in Hole 670. It could also account for the great geometrical variability of the spinel-orthopyroxene foliation and lineation through the hole. Indeed, the repeated changes in dip of these structures, in less than 100 m (Fig. 2D), could result from block tilting along cataclastic or serpentinized shear zones, during the emplacement of the peridotites in the uppermost lithosphere. An alternative explanation for this geometrical variability is of course that Hole 670 was drilled in a heap of dekametric blocks, fallen down the slope of the western ridge flank. This alternative explanation still requires the uplift of the serpentinites onto the seafloor.

Karson et al. (1987) suggested that the serpentinites of the MARK area have been uplifted during a phase of purely tectonic (amagmatic) spreading, leading to the stretching of the crust along low angle normal faults. A similar model was previously developed by Dick et al. (1981) and Karson and Dick (1984) to explain the emplacement of gabbros on the seafloor in the active corner of the Kane Fracture Zone.

In the alternative model, developed by Bonatti and Honnorez (1976) and Francis (1981), serpentinite diapirism is the leading mechanism of the emplacement of deep crustal and upper mantle rocks on the seafloor.

The petrostructural data presented in this paper does not alone provide critical evidence for, or against, one of these models. Specifically, the possible existence of intervals of sheared serpentinite at Site 670 is not evidence for the serpentinite diapirism model, as serpentinites may of course also be sheared along normal faults. Gravity and seismic surveys (Dubois et al., in prep.; Detrick et al., in prep.) may prove to be more powerful tools to discriminate between the two models. However, low to moderate angle normal faults have actually been observed in the gabbros and peridotites of the western wall of the ridge valley in the MARK area, using the *Alvin* (Dick et al., 1981; Karson and Dick, 1984) and *Nautile* (Karson et al., 1988; Cannat et al., 1988) submersibles. We therefore favor an emplacement model involving the tectonic thinning of the crust of the MARK area. We further propose that, in a context of slow spreading

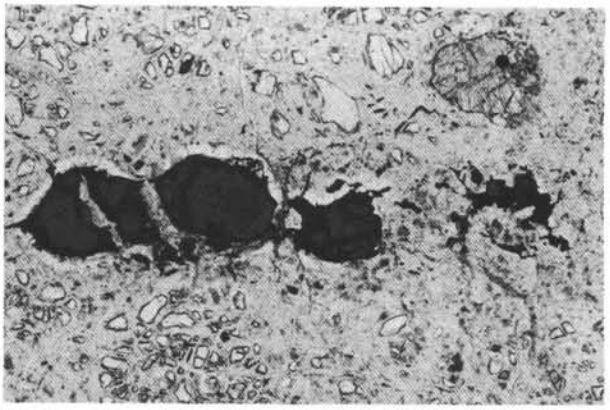

A

1 mm

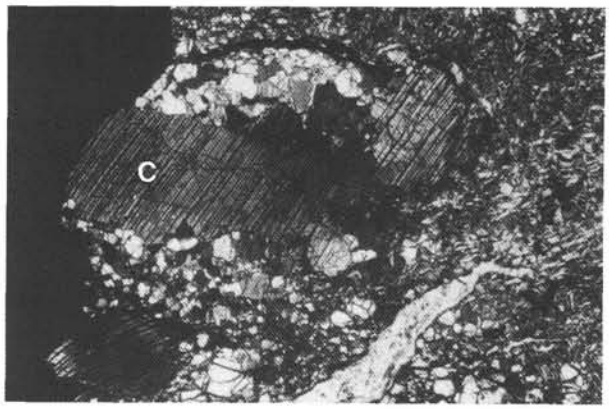

D

1 mm

B

0.5 mm

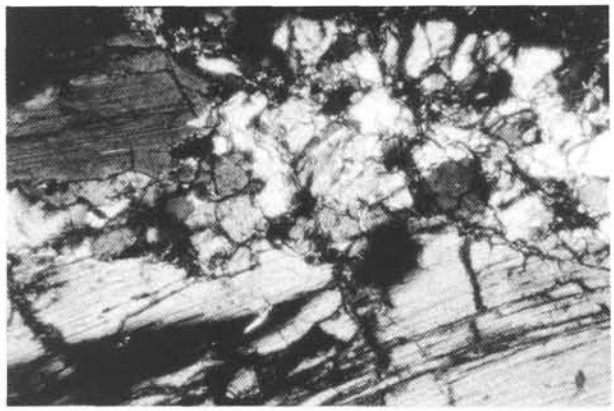

C

0.15 mm

E

20 μm

Figure 4. Photomicrographs from Hole 109-670A. **A.** Rounded spinel grain, elongated in the foliation of serpentinized harzburgite Sample 5R-2 (92–94 cm); plane light. **B.** "Retort-shaped" orthopyroxene in serpentinized harzburgite sample 8R-1 (2–4 cm); see Figure 6B for significance of numbers; crossed nicols. **C.** Recrystallized orthopyroxene in serpentinized harzburgite Sample 5R-1 (2–6 cm); crossed nicols. **D.** Recrystallized clinopyroxene, orthopyroxene, and olivine in highly deformed serpentinized harzburgite 6R-1 (49–51 cm); partly recrystallized clinopyroxene porphyroclast (C); crossed nicols. **E.** Dislocation walls in a decorated olivine (see text) of serpentinized harzburgite 8R-1 (2–4 cm); plane light. **F.** Lenses of interstitial clinopyroxene (dark bands) in serpentinized harzburgite 4W-1 (27–30 cm); these lenses are parallel to the (100) cleavage of nearby orthopyroxenes (O), which materialize the shear plane (see text); crossed nicols. **G.** Detail of the clinopyroxene lenses in Sample 4W-1 (27–30 cm); the clinopyroxene grains, partly amphibolitized, appear as grey interstitial patches in the surrounding serpentinized olivine; plane light. **H.** "Holly-leaf" type spinel in serpentinized harzburgite 5R-2 (142–145 cm); the spinel is slightly elongated in the sample's foliation, and locally intergrown with orthopyroxene (O); plane light. **I.** Websterite, Sample 9R-1 (19–20 cm); the orthopyroxene and clinopyroxene porphyroclasts are kinked, and partly recrystallized; crossed nicols.

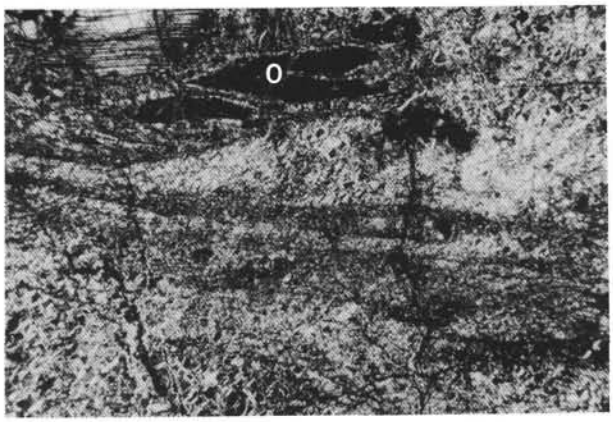

F 2 mm

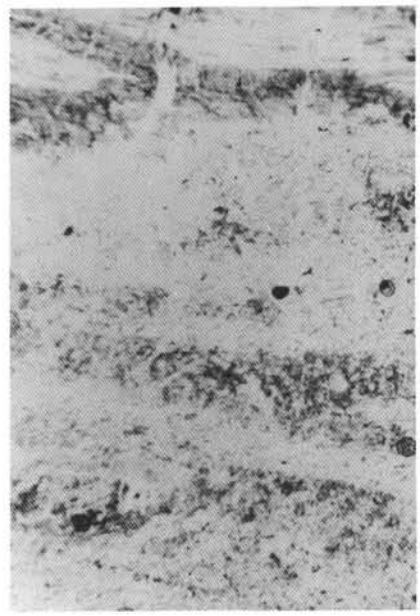

G 1 mm

H 2 mm

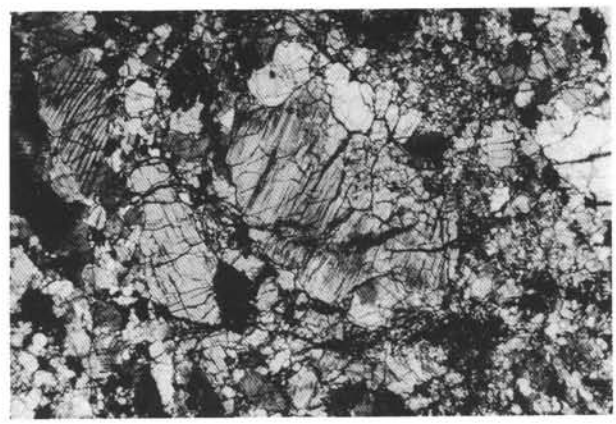

I 2 mm

Figure 4 (continued).

and discontinuous magma supply, the magmatic crust may locally be very thin, allowing normal faults with moderate offsets to bring upper mantle peridotites to the surface. This model does not exclude serpentinite diapirism during the last stages of the emplacement process, as faults and fractures allow seawater to circulate through the thinned crust, into the mantle peridotite.

Compared with the peridotites drilled 100 km to the west during Leg 45 (Site 395; Shipboard Scientific Party, 1979), the Site 670 peridotites appear more strongly strained during the plastic deformation episode. The peridotites from the two sites have otherwise similar deformation histories (Boudier, 1979). Petrographically, we note at both sites the absence of feldspar, and the abundance of clinopyroxene in the peridotites (Arai and Fujii, 1979; Sinton, 1979; Boudier, 1979). In Site 395, the magmatic twins of a clinopyroxene grain suggest that it crystallized from a circulating melt (Boudier, 1979). Our microstructural observations lead us to propose a similar origin for the interstitial clinopyroxene of the Site 670 peridotite. The crystallization of a websterite in Core 9 of Hole 670 also suggests melt circulation in the Leg 109 peridotites before the end of the plastic deformation. This hypothesis is further discussed in Juteau et al. (this volume), in view of the mineralogical data.

REFERENCES

Arai, S., and Fujii, T., 1979. Petrology of ultramafic rocks from Site 395. *In* Melson, W. G., Rabinowitz, P. D., et al.. *Init. Repts. DSDP*, 45; Washington (U.S. Govt. Printing Office), 587–594.

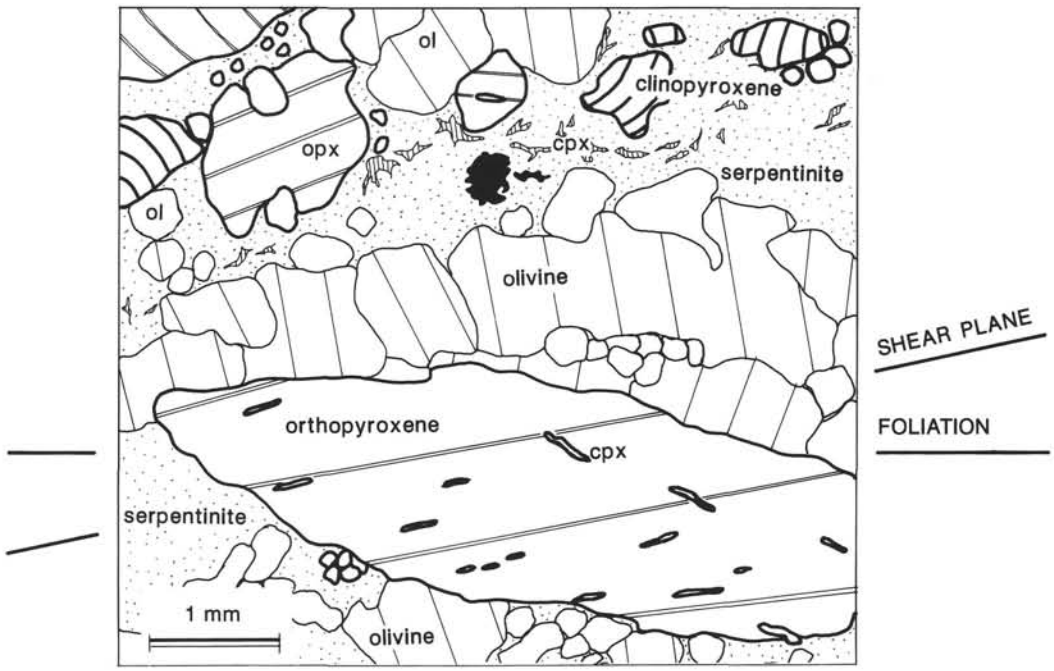

Figure 5. Sketch of the microstructure of serpentinized harzburgite Sample 109-670A-8R-1 (2–4 cm). The trace of the foliation is defined by the mean elongation of the primary minerals, and the shear plane is materialized by the (100) cleavage in orthopyroxenes.

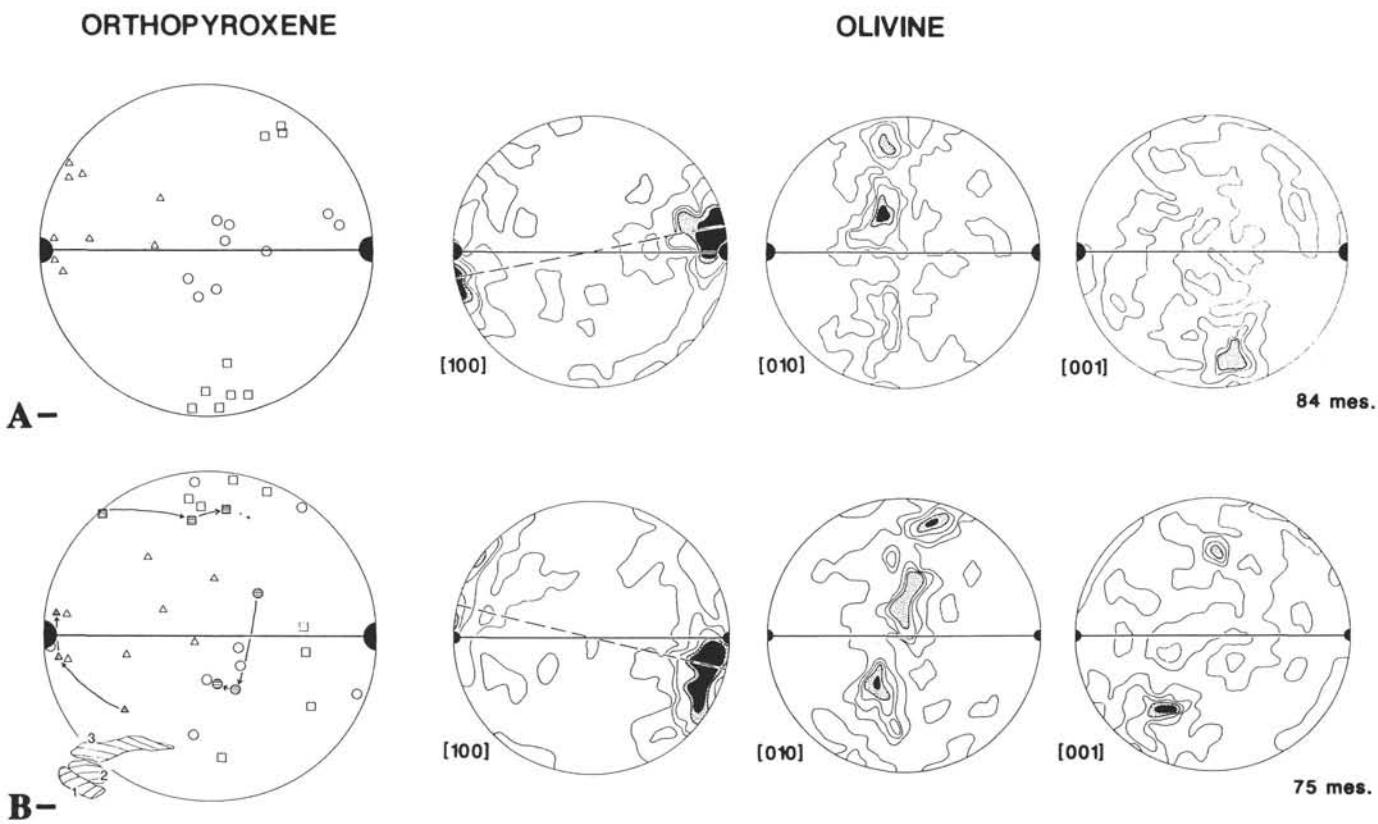

Figure 6. Olivine and orthopyroxene preferred orientation in the serpentinized peridotites in Hole 109-670A. Lower hemisphere, equal area projection. Horizontal line = foliation; black dots = lineation; dashed line = shear plane. In the orthopyroxene fabrics, the [001] axes are triangles, the [010] axes are circles, and the [100] axes are squares. In the olivine fabrics, the contours correspond to concentrations of 1.2%, 3.5%, 6%, 8.5%, 10.5%, and more, per 0.45% area. **A.** Serpentinized harzburgite 4W-1 (27–30 cm). **B.** Serpentinized harzburgite 8R-1 (2–4 cm); the rotation of the crystallographic orientation of orthopyroxene corresponds to the "retort-shaped" crystal shown in inset, and in Figure 4**B**.

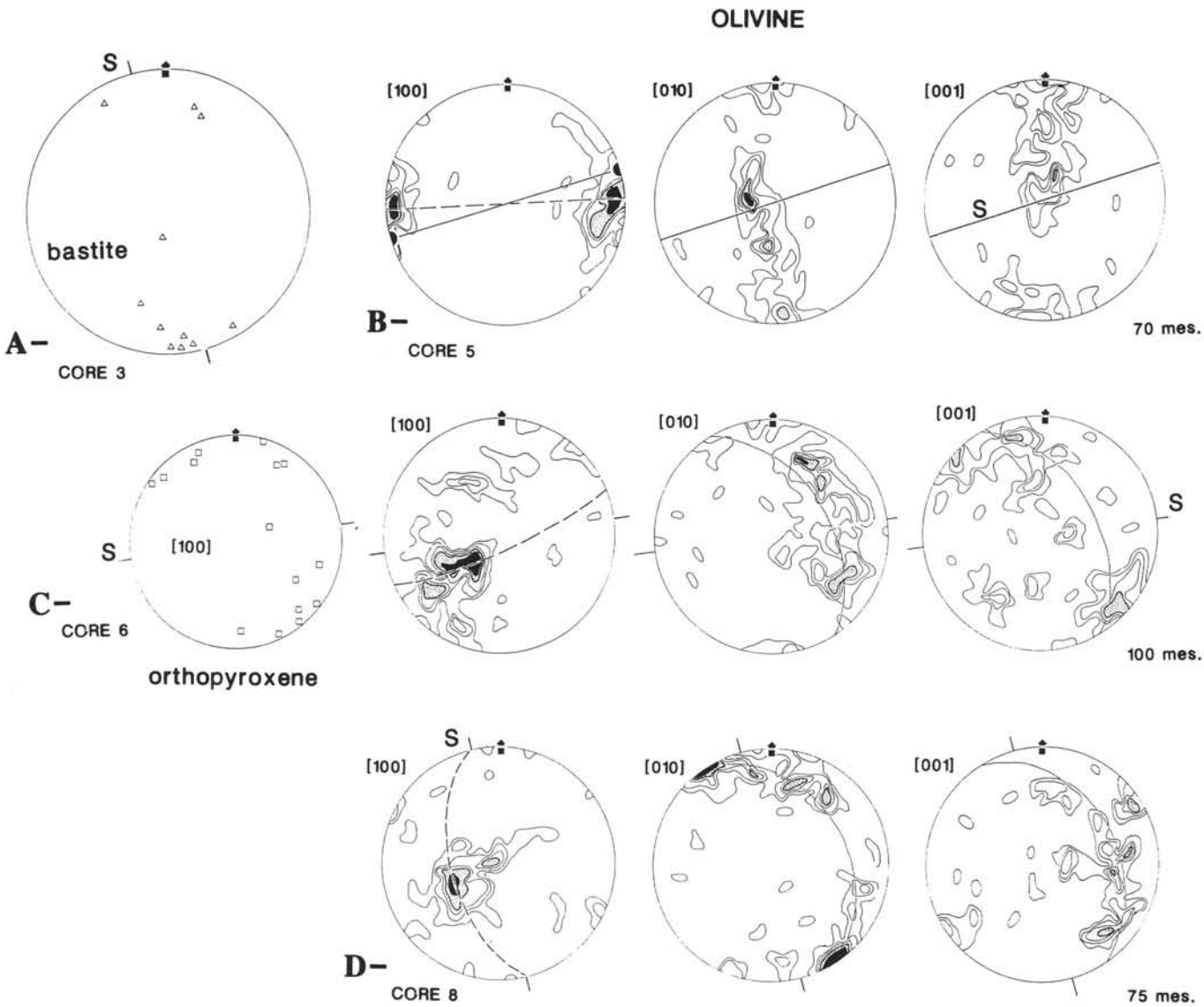

Figure 7. Mineral preferred orientation in the "oriented" samples of Hole 109-670A. Lower hemisphere, equal area projection. All diagrams are in a vertical plane, black arrow upward. **A.** Serpentinized harzburgite 3W-1 (12–14 cm); triangles = greatest refractive index of the serpentine (long axis of the serpentine fibers) in the bastite pseudomorphs; S = trace of the foliation in the thin section. **B.** Serpentinized harzburgite 5R-2 (102–104 cm); olivine preferred orientation; solid line = foliation; black dots = lineation; dashed line = shear plane; contours = 1.4%, 2.8%, 4.3%, 5.7%, 8.6%, and more, per 0.45% area. **C.** Serpentinized harzburgite 6R-1 (4–6 cm); olivine and orthopyroxene preferred orientations; S = trace of the foliation in the thin section; dashed line = shear plane; solid line = best girdle defined by the [010] and [001] axes in olivine; contours = 1%, 2%, 3%, 4%, 6%, and more, per 0.45% area. **D.** Serpentinized harzburgite 8R-1 (31–34 cm); olivine preferred orientation; S = trace of the foliation in the thin section; dashed line = shear plane; solid line = best girdle defined by the [010] and [001] axes; contours = 1.3%, 2.6%, 4%, 5.3%, 8%, and more, per 0.45% area.

Bonatti, E., and Honnorez, J., 1976. Sections of the earth's crust in the Equatorial Atlantic. *J. Geophys. Res.*, 81:4104–4116.

Bouchez, J. L., Lister, G. S., and Nicolas, A., 1983. Fabric asymmetry and shear sense in movement zones. *Geol. Rundschau*, 72:401–419.

Boudier, F., 1979. Microstructural study of three peridotite samples drilled at the western margin of the mid-Atlantic ridge. *In* Melson, W. G., Rabinowitz, P. D., et al.. *Init. Repts. DSDP 45*, Washington (U.S. Govt. Printing Office), 603–608.

Boudier, F., and Nicolas, A., 1972. Fusion partielle gabbrïque dans la lherzolite de Lanzo (Alpes piémontaises). *Bull. Suisse Mineral. Petrol.*, 52:39–56.

Cannat, M., Mevel, C., Auzende, J-M., Dubois, J., Fouquet, Y., Gente, P., and Karson, J. A., 1988. Serpentinized upper mantle on the median valley walls of the MARK area: geology and geophysics from Nautile. *EOS*, 69:1431.

Cormier, M. H., Detrick, R. S., and Purdy, G. M., 1984. Anomalously thin crust in oceanic fracture zones: new seismic constraints from the Kane Fracture Zone. *J. Geophys. Res.*, 89:10249–10266./

Detrick, R. S., and Purdy, G. M., 1980. Crustal structure of the Kane Fracture Zone from seismic refraction studies. *J. Geophys. Res.*, 85:3759–3777.

Dick, H.J.B., Thompson, G., and Bryan, W. B., 1981. Low angle faulting and steady-state emplacement of plutonic rocks at ridge-transform intersections. *EOS*, 62:406.

Durham, W. B., Goetze, C., and Blake, B., 1977. Plastic flow of oriented single crystals of olivine. 2 – Observations and interpretations of the dislocation structures. *J. Geophys. Res.*, 82:5755–5770.

Etchecopar, A., 1974. Simulation par ordinateur de la déformation progressive d'un agrégat cristallin. [Ph.D. dissert.]. Université de Nantes.

Francis, T. G., 1981. Serpentinization faults and their role in the tectonics of slow spreading ridges. *J. Geophys. Res.*, 86:11616–11622.

Goetze, C., 1975. Sheared lherzolites from the point of view of rock mechanics. *Geology*, 3:172–173.

Gueguen, Y., and Darot, M., 1980. Microstructures and stresses in naturally deformed peridotites. *Rock Mech.*, 9:159–172.

Gueguen, Y., and Nicolas, A., 1980. Deformation of mantle rocks. *Ann. Rev. Earth Plan. Sci.*, 8:119–144.

Jaoul, O., Gueguen, Y., Michaut, M., and Ricoult, D., 1979. A technique for decorating dislocations in forsterite. *Phys. Chem. Mineral.*, 5:15–20.

Karson, J. A., and Dick, H.J.B., 1984. Deformed and metamorphosed oceanic crust on the Mid-Atlantic Ridge. *Ofioliti*, 9:279–302.

Karson, J. A., Thompson, G., Humphris, S. E., Edmond, J. M., Bryan, W. B., Winters, A. T., Brown, J. R., Pockalny, R. A., Casey, J. F., Campbell, A. C., Klinkhammer, G. P., Palmer, M. R., Kinzler, R., and Sulanowska, M. M., 1987. Along axis variations in seafloor spreading in the MARK Area. *Nature*, 328:681–685.

Karson, J. A., Mevel, C., Auzende, J-M., Cannat, M., Dubois, J., Fouquet, Y., and Gente, P., 1988. Extensional structures on the W median valley wall and nodal basin in the MARK area. *EOS*, 69:1431.

Kirby, S. H., 1985. Rock mechanics observations pertinent to the rheology of the continental lithosphere and the localization of strain along shear zones. *Tectonophysics*, 119:1–27.

Kohlstedst, D. L., Goetze, C., Durham, W. B., and Vander Sande, J., 1976. New technique for decorating dislocations in olivine. *Science*, 191:1045–1046.

Komor, S. C., Elthon, D., and Casey, J. F., 1985. Serpentinization of cumulate ultramafic rocks from the North Arm Mountain massif of the Bay of Islands ophiolite. *Geochim. Cosmochim. Acta*, 49:2331–2338.

Le Sueur, E., Boudier, F., Cannat, M., Ceuleneer, G., and Nicolas, A., 1984. The Trinity mafic-ultramafic complex: first results of the structural study of an untypical ophiolite. *Ofioliti*, 9:487–498.

Mercier, J. L., and Nicolas, A., 1975. Textures and fabrics of upper mantle peridotites as illustrated by xenoliths from basalts. *J. Petrol.*, 16:454–487.

Mercier, J. L., Anderson, D. A., and Carter, N. L., 1977. Stress in the lithosphere : inferences from steady state flow of rocks. *Pure Appl. Geophys.*, 115:199–226.

Nicolas, A., 1969. Serpentinisation d'une lherzolite: bilan chimique, implication tectonique. *Bull. Volcanolog.*, 32:499–508.

Nicolas, A., and Poirier, J. P., 1976. *Crystalline plasticity and solid-state flow in metamorphic rocks*. New York (Wiley), 444 p.

Nicolas, A., and Jackson, M., 1982. High temperature dikes in peridotites: origin by hydraulic fracturing. *J. Petrol.*, 23:568–582.

Post, R. L., 1977. High-temperature creep of Mt. Burnet dunite. *Tectonophysics*, 42:75–110.

Ross, J. V., Ave Lallemant, H. G., and Carter, N. L., 1980. Stress dependence of recrystallized grain and subgrain size in olivine. *Tectonophysics*, 70:39–61.

Shipboard Scientific Party, 1979. Sites 395 and 395A. *In* Melson, W. G., Rabinowitz, P. D., et al.. *Init. Repts. DSDP*, 45; Washington (U.S. Govt. Printing Office), 131–264.

Sinton, J. M., 1979. Petrology of alpine-type peridotites from Site 395, DSDP Leg 45. *In* Melson, W. G., Rabinowitz, P. D., et al.. *Init. Repts. DSDP*, 45: Washington (U.S. Govt. Printing Office), 595–601.

Date of initial receipt: 21 March 1988
Date of acceptance: 28 April 1989
Ms 106/109-118